Int J Fract (2021) 231:61–77
https://doi.org/10.1007/s10704-021-00564-5

ORIGINAL PAPER

Influence of polishing technique on crack resistance of quartz plates

Vasilina A. Lapitskaya · Tatyana A. Kuznetsova · Andrei L. Khudoley · Anastasiya V. Khabarava · Sergei A. Chizhik · Sergei M. Aizikovich · Evgeniy V. Sadyrin

Received: 1 April 2021 / Accepted: 23 June 2021 / Published online: 10 July 2021

Abstract The sensory properties of monocrystalline quartz are influenced by its surface, mechanical properties, and crack resistance. The surface quality of quartz is significantly influenced by its processing technology. The aim of this work is comparative studies of surface morphology, roughness, mechanical properties, and crack resistance of single-crystal quartz plates after chemical–mechanical and magnetorheological polishing. Surface morphology was assessed by atomic force microscopy (AFM). E and H were determined by nanoindentation (NI). The fracture toughness was assessed by the indentation method with visualization of the AFM imprint topography. The task was to determine the most reliable method for calculating the critical stress intensity factor K_{IC} for quartz, adequate to the load range from 0.01 to 0.5 N. It was found that chemical–mechanical polishing creates an altered layer 70 nm thick on the quartz surface, which significantly changes its mechanical properties and K_{IC}.

V. A. Lapitskaya · T. A. Kuznetsova ·
A. V. Khabarava · S. A. Chizhik
Nanoprocesses and Technology Laboratory, A.V. Luikov Heat and Mass Transfer Institute of the National Academy of Science of Belarus, 15, P. Brovki str, 220072 Minsk, Belarus

A. L. Khudoley
High-Precision Surfacing Laboratory, A.V. Luikov Heat and Mass Transfer Institute of the National Academy of Science of Belarus, 15, P. Brovki str, 220072 Minsk, Belarus

S. M. Aizikovich · E. V. Sadyrin (✉)
Research and Education Center "Materials", Don State Technical University, 1 Gagarin Sq., Rostov-on-Don, Russia 344003
e-mail: e.sadyrin@sci.donstu.ru

Graphic abstract

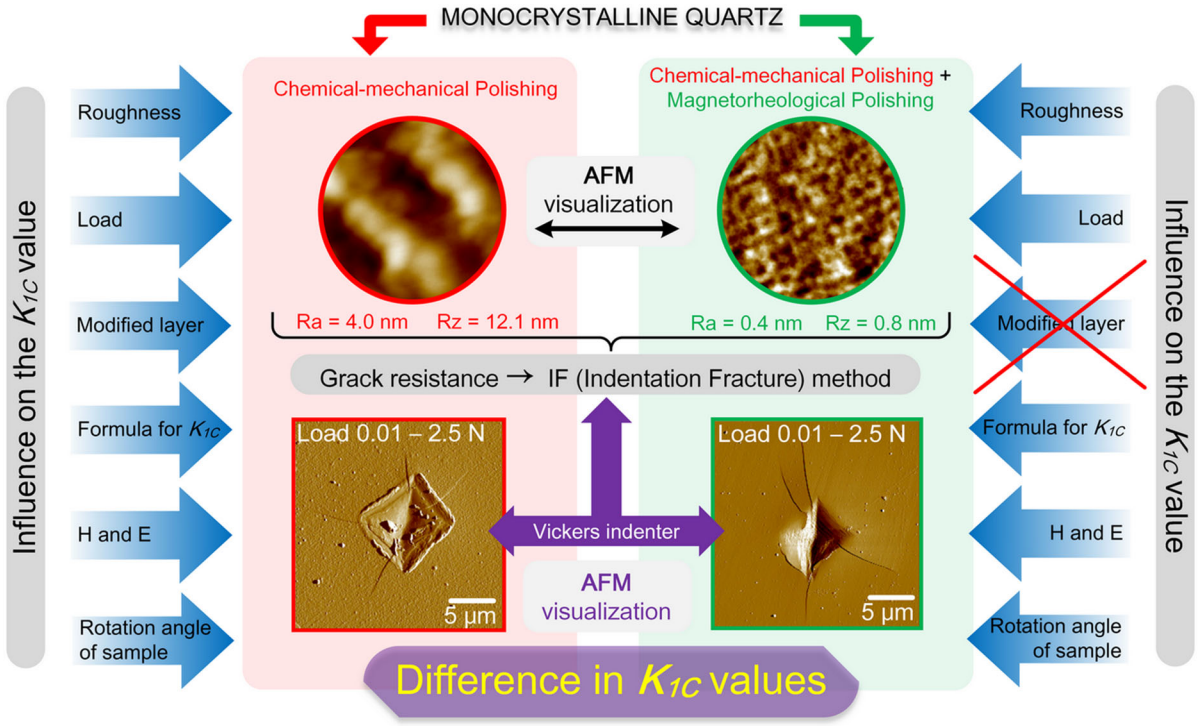

Keywords Quartz · Fracture toughness · Nanoindentation · Atomic force microscopy · Chemical–mechanical polishing · Magnetorheological polishing

1 Introduction

Monocrystalline quartz is a multifunctional material with special optical, piezoelectric, and thermophysical properties (Baek et al. 2018; Trukhin 2019; Yang et al. 2018; Molaei and Siavoshi 2020). It is used for elements of precision optics, resonators, accelerometers, gyroscopes, as substrates for microelectronics (Danel and Delapierre 1991; Lee et al. 2018; Yu et al. 2018; Beitia et al. 2015; Matko and Milanovich 2019; Bai et al. 2020). One of the most effective sensors based on monocrystalline quartz is quartz crystal micro- and nanobalance (QCM and QCN) (Hampitak et al. 2020; Rudolph et al. 2021). The quality and level of roughness can degrade the properties of sensitive elements based on quartz crystals. For example, a decrease in roughness from 600 to 2 nm leads to a proportional decrease in the frequency shift and QCM scattering (Cho et al. 2007). The sensitivity of the recognition layers of biosensors is largely determined by their thickness and surface roughness of a quartz crystal (Rianjanu et al. 2019; Leppin et al. 2020; Dong et al. 2019). Such a sensor element requires high-precision processing to a roughness comparable to the parameters of the crystal lattice. Roughness affects not only the recognizing properties of the deposited layers—it is interrelated with the characteristics of crystal vibrations in some surface modes (Hao et al. 2018). To obtain surfaces with a certain roughness, various techniques are used: chemical–mechanical (Xia et al. 2020), laser (Hildebrand et al. 2011; Weingarten et al. 2017), magnetorheological (Cao et al. 2019; Bedi and Singh 2016; Gorodkin and Novikova 2012), chemical (Bo et al. 2014), ion-beam (Zhou et al. 2019), ultrasonic abrasive (Guzzo et al. 2003), combined methods (Gupta et al. 2020; Zhong 2008) and others.

To control the surface roughness of optical and piezoelectric materials, in particular quartz crystals, non-contact optical profilometry and atomic force microscopy (AFM) are common methods (Cho et al. 2007; Dokou et al. 2002; Lapitskaya et al. 2020; Kuznetsova et al. 2020). Optical non-contact profilometry usage provides fast scanning of relatively big areas of interest (Sadyrin et al 2020b; Burlakova et al. 2019), but it's can give incorrect roughness values due to the influence of the optical properties of the material and the phenomena of reflection and absorption of light. AFM, due to the high accuracy of direct measurement of surface topography, makes it possible to determine roughness with angstrom accuracy (Misumi et al. 2019; Anishchik et al. 2005; Warcholinski et al. 2019).

Any polishing leads to changes in the properties of the surface layers of the material (Kanaev 2019) and in sensitive MEMS technologies the degree of this change must be taken into account. Mechanical polishing can lead to weakening / hardening of the surface layer of the material and formation of the smear layer (Sadyrin et al. 2020a). Laser polishing, due to high temperatures, can lead to phase transitions in the material (Ma et al. 2017). Polishing using focused ion beam is time and resource consuming technique, moreover it poses serious limitations on the sample size (Malshe et al. 1999; Vasiliev et al. 2018). Ultrasonic abrasive polishing is often conducted by skillful handwork, thus the process becomes time-consuming and not well accepted concerning the reliability of the polished surface (Hocheng and Kuo 2002). Among all types of polishing, the most promising is magnetorheological one, which provides the smallest size and number of micro-roughnesses among other methods (Cao et al. 2019; Bedi and Singh 2016; Gorodkin and Novikova 2012; Kim et al. 2009).

Mechanical properties of quartz play a significant role in the QCN design, especially taking into account the decrease in their size and thinning of the sensitive elements (Singh 2016; Liang et al. 2015). The mechanical properties affect the electromechanical coupling coefficient, which is important for the recognition functions of quartz elements (Lamberson and Ramesh 2017). The good resistance of quartz structures to vibrations, shocks and other influences directly depends on its crack resistance. Crack resistance of the material is characterized by the critical stress intensity factor K_{IC} (Lapitskaya et al. 2019). The indentation method is widely used to determine K_{IC} in elements of microtechnology and silicon wafers (Ferguson et al. 1987; Guzzo 2001). The accuracy of K_{IC} determination depends on the accuracy of visualization of the formed cracks.

The aim of the present research was to carry out comparative studies of surface morphology, roughness, mechanical properties, and crack resistance of AT-cut quartz crystals after chemical–mechanical and magnetorheological polishing. AFM was used to increase the accuracy of determining the surface morphology and crack resistance by indentation method for visualizing the surface topography in the initial state and with an imprint and cracks.

2 Materials and methods

2.1 Sample preparation

As an object of research, we took quartz elements—two AT-cut (or yxl/+ 35° cut) plates of crystalline quartz with a diameter of 12 mm and a thickness of 3 mm, which are mass-produced and are widely used in the manufacture of precision resonators and complex filters for devices for stabilization and frequency selection. Initially, both plates were processed by chemical–mechanical polishing (CMP), then one of them was additionally subjected to magnetorheological polishing (MRF). The CMP was produced with a flat polisher using a slurry containing free abrasive cerium oxide. The MRF was carried out on a 5-axis CNC machine (ITMO, Minsk, Belarus) with a small-sized magnetically controlled tool using a water-based polishing liquid with the addition of a nano-diamond abrasive. The amount of material removed from the quartz surface during MRF processing was at least 2 μm to ensure the removal of the damaged layer formed after CMP and the performance of previous operations.

2.2 Experimental procedures

Crack resistance was determined by the indentation method. Three imprints were made on each of the plates at different loads using a PMT-3 microhardness tester (LOMO, St. Petersburg, Russia). A Vickers tip was used as an indenter. The load on the indenter varied from 0.01 to 2.5 N. In our work, we used AT-

cut (or cut yxl/+ 35°) monocrystalline quartz. During the manufacture of monocrystalline quartz plates, the orientation on them is not indicated in any way. Therefore, in this work, we evaluated the influence of anisotropy on the value K_{IC} by rotating the crystal during indentation. The effect of the angle of rotation of the quartz plate relative to the indenter (initial 0°, 45°, and 90°) on the shape of the imprint, the type and length of cracks, and the magnitude of crack resistance were obtained. Different orientations of the specimen were used in order to exclude the influence of the orientation of the quartz plate on the values of crack resistance. When processing the data for calculating K_{IC} the direction of the largest total crack length was chosen. The comparison was carried out at a load of 1.5 N.

A Dimension FastScan AFM (Bruker, Santa Barbara, State of California (CA), USA) in PeakForce quantitative nanoscale mechanical mapping mode with a standard silicon cantilever type NSC-11 (Mikromasch, Tallinn, Estonia) with a radius of curvature of the probe tip of 10 nm and a console rigidity of 4.89 N/m was used to visualize imprints and cracks, to quantify adhesion forces and surface roughness (Khort et al. 2020; Lapitskaya et al. 2018; Kuznetsova et al. 2018; Nikolaev et al. 2020). Determination of the surface roughness of the samples was carried out in the semi-contact mode according to ISO 19606:2017. Scanning fields were as follows: 91.8 × 91.8, 10 × 10 and 1 × 1 μm^2. The measurements were carried out in 3 different areas of the sample at a distance of about 2 mm from each other. Resolution of the scanning frame was 512 × 512 points. Measurement errors for the axes were as follows: XY: ± 0.2 nm, for Z: ± 0.03 nm. The adhesion force was determined by the maximum force of separation of the cantilever tip from the surface of the samples from the force curves of the "approach-withdrawal".

Microhardness H, Young's modulus E, and deformation η (plastic and elastic components of deformation) of quartz were determined using nanoindentation (NI) technique on a Hysitron 750 Ubi NI device (Bruker, Minneapolis, MN, USA) equipped with a Berkovich diamond indenter with a radius of curvature of 150 nm for continuous recording of deformation curves. As a result, data on the applied load and the corresponding indentation depth was obtained as a function of the dependence $F = f(h_{Ber})$. The load was 10 mN. Additionally, studies of microhardness and modulus of elasticity by depth were carried out at a load ranging from 0.2 to 5.0 mN. Elastic recovery η_{elast} and plastic deformation η_{plast} were calculated from the shape of the deformation curves $F = f(h_{Ber})$ (Jha et al. 2012). The mechanical work $W_{totalal}$, performed during indentation was only partially spent on plastic deformation W_{plast} (Jha et al. 2012). When the applied load was removed, part of the work (the work of elastic deformation W_{elast}) was released. Formula (1) contains information characterizing the plastic properties of the test specimen:

$$\eta_{elast} = \frac{W_{elast}}{W_{total}}, \tag{1}$$

where $W_{tolal} = W_{elast} + W_{plast}$.

The plastic component was calculated as

$$\eta_{plast} = (1 - \eta_{elast}) \cdot 100\% \tag{2}$$

To determine K_{IC} several formulas were used to check the correctness of the obtained values and the influence of the parameters included in the formulas on the values K_{IC} (Sergejev 2006; Lawn and Fuller 1975; Evans and Wilshaw 1976; Niihara et al. 1982; Niihara 1983):

$$K_{IC} = 0.0515 \frac{P}{c_1^{\frac{3}{2}}}, \tag{3}$$

$$K_{IC} = 0.079 \frac{P}{a^{\frac{3}{2}}} \log\left(4.5 \frac{a}{c_1}\right) \tag{4}$$

$$K_{IC} = 0.035 \left(\frac{c_1}{a}\right)^{-\frac{1}{2}} \cdot \left(\frac{H_V}{E\Phi}\right)^{-\frac{2}{5}} \cdot \left(\frac{H_V a^{\frac{1}{2}}}{\Phi}\right) \tag{5}$$

$$K_{IC} = 0.048 \left(\frac{c_1}{a}\right)^{-\frac{1}{2}} \cdot \left(\frac{H_V}{E\Phi}\right)^{-\frac{2}{5}} \cdot \left(\frac{H_V a^{\frac{1}{2}}}{\Phi}\right) \tag{6}$$

$$K_{IC} = 0.0726 \frac{P}{c_2^{\frac{3}{2}}} \tag{7}$$

$$K_{IC} = 0.129 \left(\frac{c_2}{a}\right)^{-\frac{3}{2}} \cdot \left(\frac{H_V}{E\Phi}\right)^{-\frac{2}{5}} \cdot \left(\frac{H_V a^{\frac{1}{2}}}{\Phi}\right) \tag{8}$$

$$K_{IC} = 0.014 \left(\frac{E}{H_V}\right)^{\frac{1}{2}} \cdot \left(\frac{P}{c_2^{\frac{3}{2}}}\right) \tag{9}$$

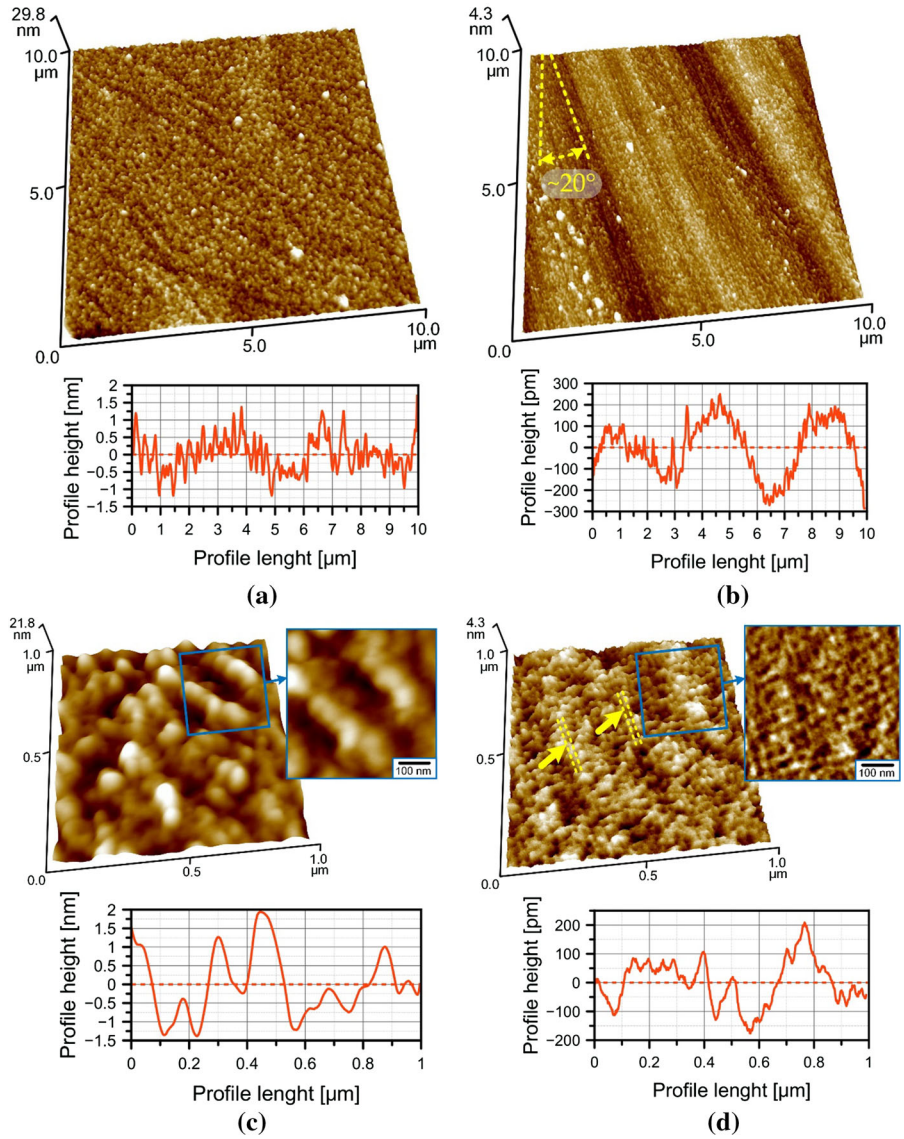

Fig. 1 AFM images of the surface morphology of quartz plates after chemical–mechanical polishing (**a**, **c**) and magnetorheological polishing (**b**, **d**) in fields of 10 × 10 (**a**, **b**) and 1 × 1 (**c**, **d**) μm^2

where P is the load on the indenter, N; c_1 is the length of the crack near the imprint, m; c_2 is the length of the crack from the center of the imprint, m; a is the length of the half-diagonal of the imprint, m; H_V is Vickers hardness, GPa; E is the modulus of elasticity, GPa; Φ is a constant, an indicator of the bond reaction in the crystal lattice, $\Phi \approx 3$.

Formulas (3)–(6) include the length of the crack near the indentation c_1, and in (7)–(9), the length of the crack from the center of the indentation c_2. For selection of the appropriate formula, the ratio c_2/a should be determined. If $c_2/a < 2.0$, then Palmquist cracks are formed in the sample and the calculation is carried out according to the formula (3)–(6) (Sergejev 2006; Lawn and Fuller 1975; Evans and Wilshaw 1976; Niihara et al. 1982); if $c_2/a > 2.0$, then median cracks are formed in the sample, and the calculation is carried out by the formulas (7)–(9) (Lawn and Fuller 1975; Niihara et al. 1982; Ebrahimi and Kalwani 1999; Lawn et al. 1980).

In the formulas (3) and (7) only the length of the crack and the applied load are taken into account and there is no dependence on the mechanical properties of the material, in (2) the length of the subdiagonal of the imprint is added to the length of the crack and the load,

in (5), (6) and (8)—all indentation parameters, crack length and mechanical properties of materials are used and there is no direct dependence on the applied load. In most formulas used earlier in the literature, loads of more than 1 N were used. In those cases when lower loads (0.25–0.75 N) were used, the values of a, c_1 and c_2 were determined inaccurately and because of this, at low loads, the difference in a,c_1, and c_2 between quartz slices of different orientations was not revealed (Guzzo 2001). The task was to select a calculation method that is most adequate for low loads (from 0.01 to 0.5 N) to obtain the correct value of $K_{IC.}$

The H_V values obtained by the NI method were used in the calculations. In this case, H was taken from the Berkovich imprint, obtained at small (1–5 mN) loads and guaranteed to be free of cracks. This approach seems to be more correct, since microhardness imprints often contain cracks that are not visible to optics.

3 Results and discussion

AFM images of the surface (fields of 10 × 10 and 1 × 1 μm^2) of quartz wafers after CMP and MRF are shown in Fig. 1. On a field of 10 × 10 μm^2, the surface after CMP looks more homogeneous, without a strongly pronounced direction (Fig. 1a). Quartz after MRF demonstrates elongated depressions oriented in one direction on the surface, there is a pronounced directionality at an angle of about 20° to the Y axis (Fig. 1b). Comparison of the surface profiles shows that the relief drop after CMP was about 5 times higher than that of quartz after MRF. After CMP, particles with a size of 100–150 nm are evenly distributed on the quartz surface (Fig. 1c).

Their formation on the surface of monocrystalline quartz is associated with the separation of small volumes of material during processing, their repeated mixing with the participation of polishing liquids.

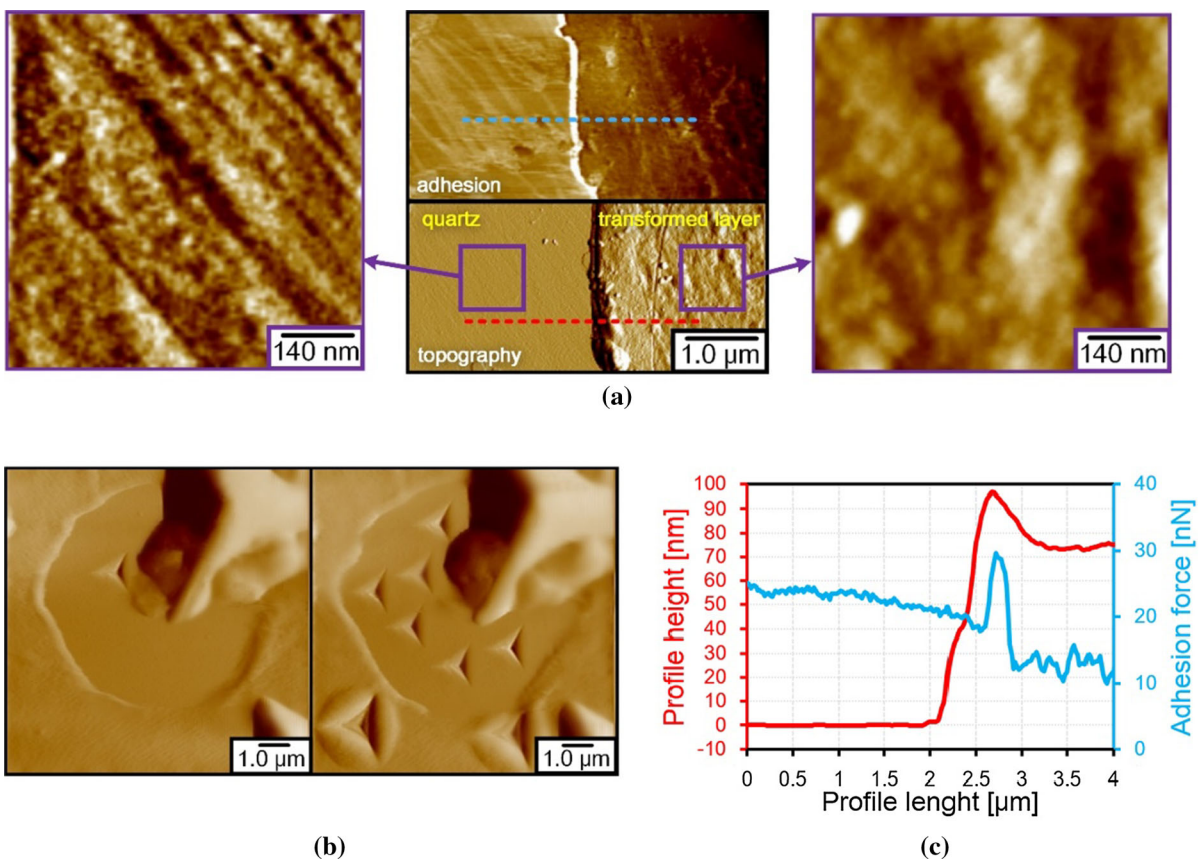

Fig. 2 The surface of a quartz plate after chemical–mechanical polishing with areas of damage to the upper layer: **a**, **c** morphology obtained on AFM and surface profile, respectively; **b** morphology obtained on NI

Table 1 Roughness, physical and mechanical properties of quartz plates after various polishing techniques

Parameter	Polishing type		
	Chemical–mechanical (*CMP*)		Magnetorheological (*MRF*)
	With layer	Without layer	
Ra (nm)	4.0 ± 0.2	1.6 ± 0.1	0.4 ± 0.02
Rq (nm)	10.1 ± 0.5	3.8 ± 0.2	0.6 ± 0.03
Rz (nm)	12.1 ± 0.6	2.8 ± 0.1	0.8 ± 0.04
Fad (nN)	13.07 ± 0.65	21.97 ± 1.10	15.90 ± 0.79
E (GPa)	88 ± 7	101 ± 1	99 ± 1
H (GPa)	8.7 ± 2.4	13.7 ± 0.1	13.5 ± 0.1
H/E	0.10	0.14	0.14
η_{plast} (%)	30.7 ± 3.1	22.6 ± 0.2	24.7 ± 0.2
η_{elast} (%)	69.3 ± 6.9	77.4 ± 0.7	75.3 ± 0.8

Surface morphology significantly depends on the type of polishing and the used abrasive and liquid during polishing (Bo et al. 2014; Dokou et al. 2002). Presence of the block (grain) structure on the surface after CMP shows that a modified layer was formed. Also, on the surface, like in quartz after CMP, particles with a size of 20–30 nm are distributed. The surface morphology (field 10 × 10 μm^2) of the quartz after MRF is similar to the morphology obtained in Zhao et al. (2018). The fine structure of quartz after MRF, revealed at a field of 1 × 1 μm^2, shows directional structure elements (Fig. 1d). Lines are visible on the surface, oriented in the same way as depressions, at an angle of about 20° to the Y axis with a period of 20 nm (Fig. 1d, arrows). The inset to Fig. 1d shows an ordered surface structure corresponding to the crystal lattice. Material carryover during MRF does not occur randomly, but according to the directions of the crystal lattice. The direction at an angle of about 20° to the Y axis in the images of the surface with large depressions obviously correspond to the direction in the quartz lattice with a longer bond length and, accordingly, weaker. In this direction, the material was removed first. The inset shows this direction and perpendicular to it. All blocks are 20–30 nm in size and oriented in a given order by the lattice. It can be safely said that the modified layer on the quartz surface after MRF is absent. The lines of preferential grooves on the quartz surface will serve as a guide for its orientation under the indenter when making imprints to determine K_{IC}.

The roughness of the surface of a quartz plate after chemical–mechanical polishing is significantly higher than after magnetorheological polishing. Ra, Rq, and Rz for quartz after MRF were 0.4, 0.6, and 0.8, respectively. The roughness values of the quartz wafer after MRF are in good agreement with (Zhao et al. 2018). On a quartz sample after CMP, the surface layer affects the roughness value: Ra, Rq, and Rz are 4.0, 10.1, and 12.1 nm, respectively, and these values correlate with the results (Yuan et al. 2003). When examining the surface morphology of the quartz plate after CMP, the sites of rupture of the altered layer were identified (Fig. 2). The layer thickness was 70–80 nm (Fig. 2c, red profile). In places of rupture, a completely different surface structure was revealed.

The roughness of a surface with open areas (without a layer) is 3–4 times less than a surface with a layer. In the mode of adhesion forces (Fig. 2a, adhesion) it was found that the quartz surface without a layer demonstrated higher values of the adhesion force compared to the surface with a layer (Fig. 2c, blue profile). The adhesion force on the surface of quartz with a layer was 13.07 nN, and without a layer—21.97 nN. On the surface of quartz without a modified layer, directional lines of grooves were also revealed, while they are deeper than in quartz after MRF.

The NI method was used to determine the physical and mechanical properties of quartz plates (Table 1). It has been established that the presence of a modified layer has a significant effect on the value of mechanical properties. NI imprints on the surface after CMP with a modified layer were twice as large as without it (Fig. 2b). The Young's modulus *E* and microhardness *H* obtained on a quartz surface without a layer were 101 ± 1 and GPa and 13.7 ± 0.1 GPa while those with a layer were 88 ± 7 GPa and 8.7 ± 2.4 GPa,

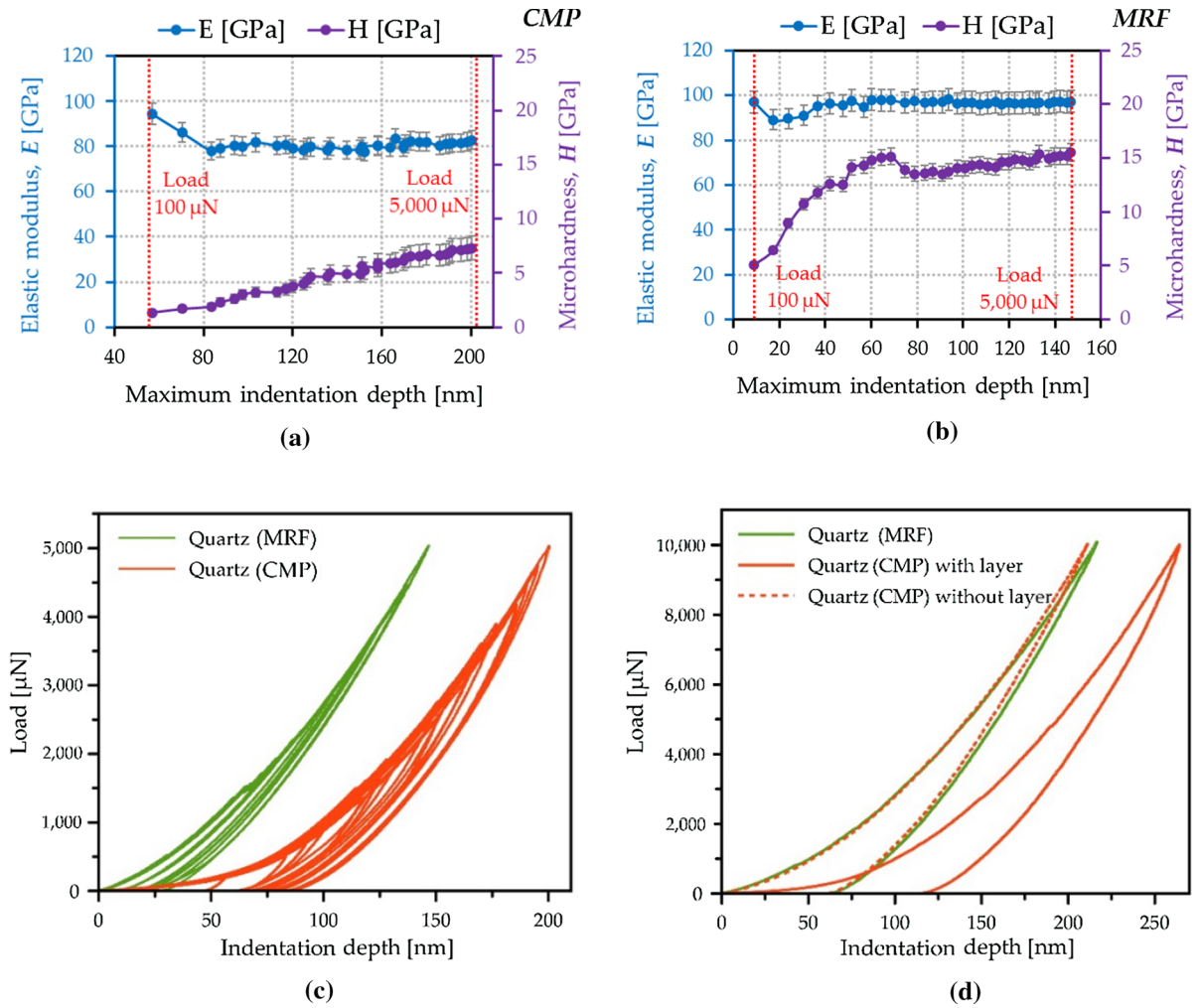

Fig. 3 Dependences of the elastic modulus and microhardness of silicon wafers on the indentation depth after CMP (**a**) and MRF (**b**) and indentation curves (**c**,**d**)

respectively. Quartz after CMP can be considered as a sample with a "soft" coating of 70–80 nm thickness. Therefore, the quartz substrate makes a significant contribution to these values. Judging by the large size of the imprints, E and H of the modified layer itself is much lower. The modulus of elasticity and microhardness of quartz after MRF are virtually the same (Table 1) as for quartz after CMP without a layer and amounted to $E = 99 \pm 1$ GPa and $H = 13.5 \pm 0.1$ GPa. The values for H and E are close to the ones obtained by the NI method in (Whitney et al. 2007; Yu et al. 2012).

According to the dependence of the modulus of elasticity and microhardness on the maximum indentation depth, it was found that under a load of 100 μN, the indentation depth for quartz after CMP was 60 nm, and for quartz after MRF—10 nm (Fig. 3a, b). With a maximum possible instrument load of 10 mN, the indentation depth for quartz after CMP is 200 nm, and for quartz after MRF it is 148 nm. Thus, the presence of a "soft" layer on the surface of the sample after CMP leads to higher values of the indentation depth. After CMP, the observed values of microhardness on the sample increase with increasing load and, accordingly, the penetration depth.

The indentation curves characterize the level of deformation (plastic and elastic) at the indentation site (Fig. 3c, d). For "soft" materials, the area under the curve is much larger and, accordingly, the plastic component of deformation is larger (Oliver and Pharr

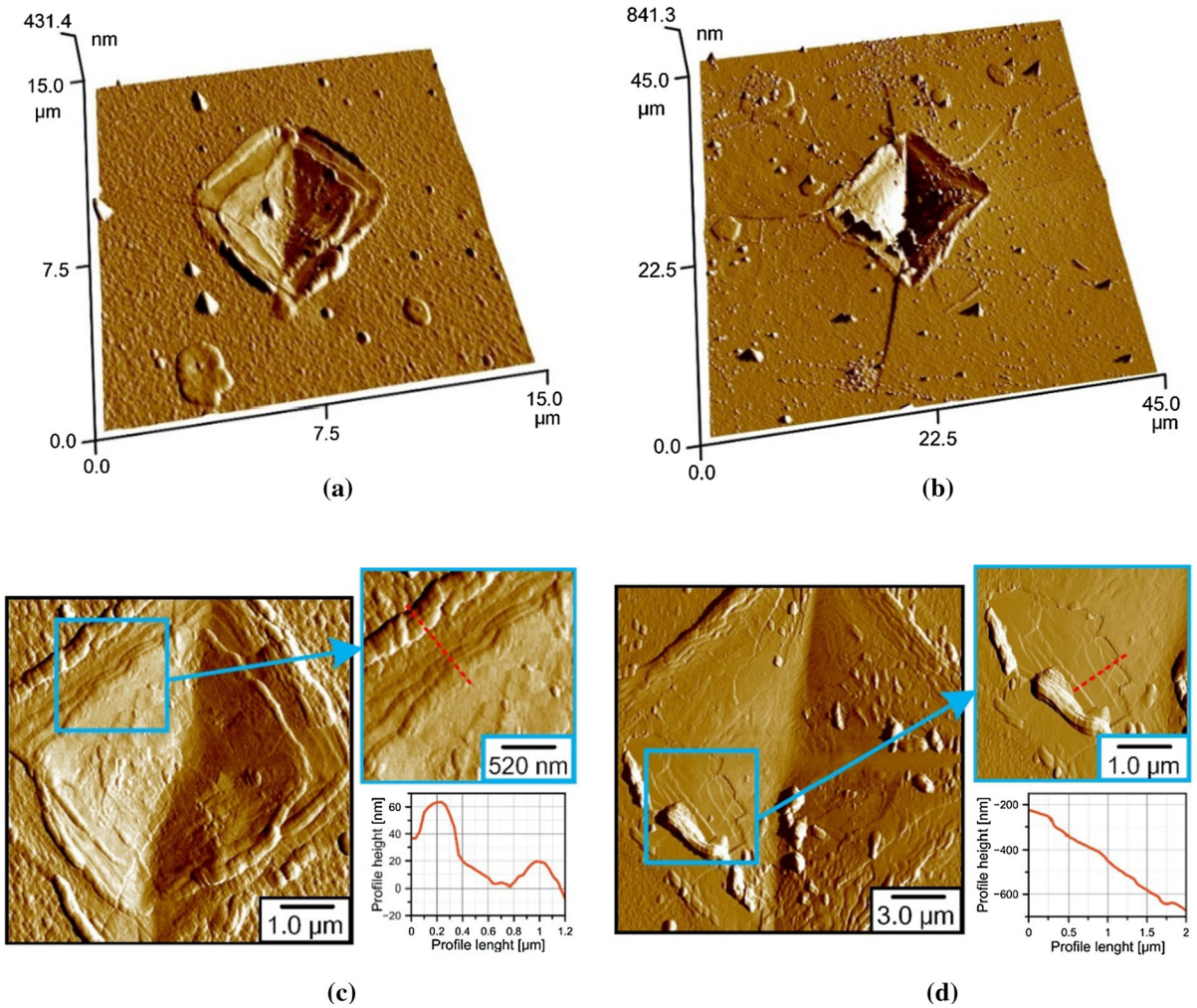

Fig. 4 AFM images of indentations at a load of 0.01 N (**a**, **c**) and 1.5 N (**b**, **d**) on quartz after chemical–mechanical polishing

1992). For "hard" materials, the elastic component of deformation is larger and the area under the curve is smaller (Oliver and Pharr 1992). The difference in modulus of elasticity at 11 GPa and microhardness at 5 GPa results in a difference in the shape of the curves for quartz after MRF and after CMP (Fig. 3c, d). The curves for quartz after MRF and for quartz after CMP without a layer coincide (Fig. 3d). For quartz after MRF, the elastic component of deformation is 75.3%, and the plastic component is 24.7%. Quartz after CMP without a layer has virtually the same values. In quartz with a layer, the plastic component increases to 30.7%, while the elastic decreases to 69.3%. The increase in the plastic component in quartz with a changed layer is explained by the shape of the curve, with a long initial section close to the X axis and a significant deflection of the curve.

The shape of Vickers imprints on the surface of quartz after CMP and MRF polishing was practically the same when visualized by optical microscopy. The contour of the imprints was not precisely defined, it is only possible to approximately determine the size of the diagonal. AFM imaging revealed a significant difference both in the shape of the contour and in the morphology of the Vickers indentation faces obtained on quartz (Figs. 4, 5). The shape of the imprints on quartz after CMP demonstrated symmetry, with smooth contour lines (Fig. 4a, b). A small bead is located along the indentation contour from the torn altered layer, the slopes of the imprint were covered

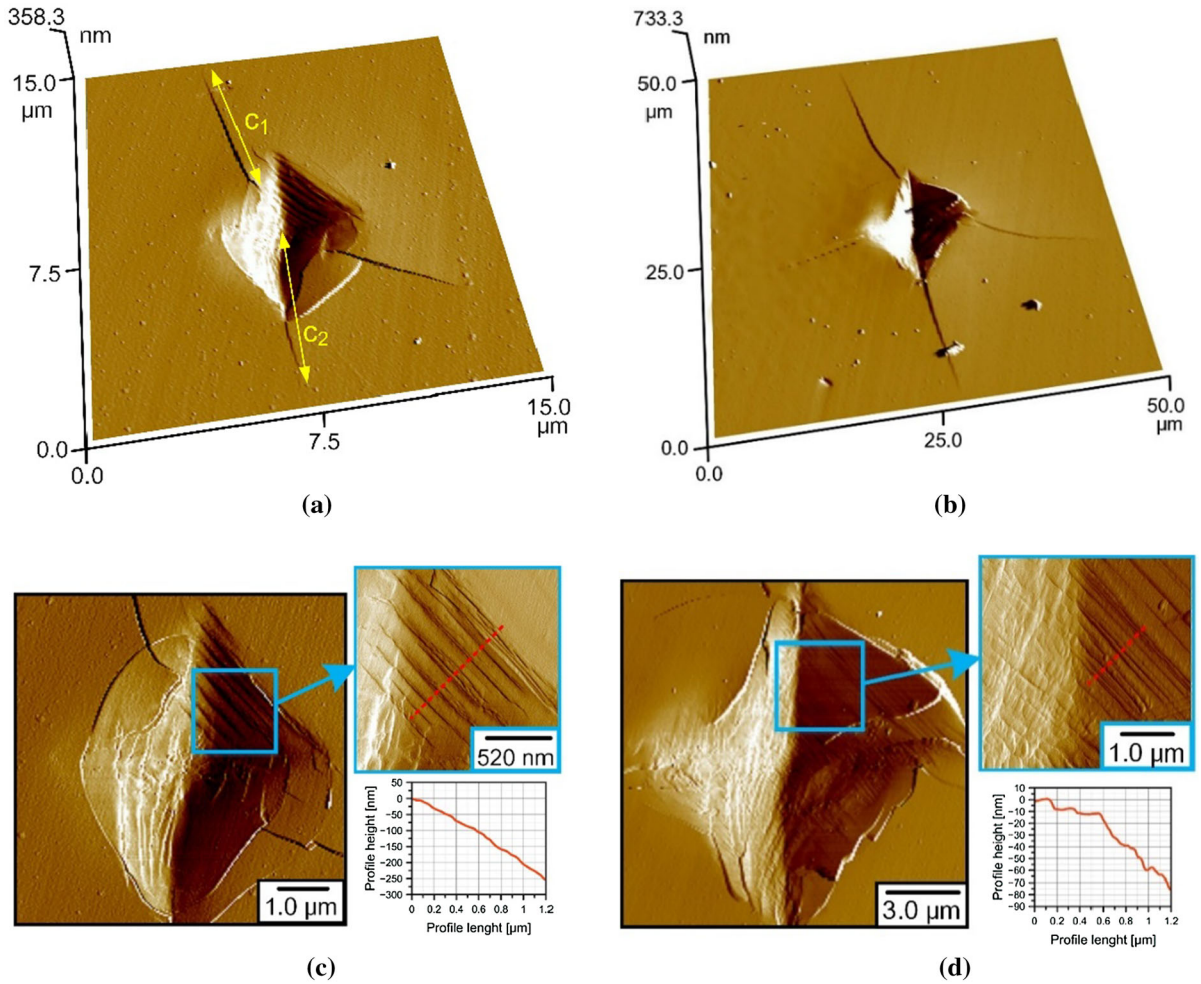

Fig. 5 AFM images of indentations under a load of 0.01 N (**a**, **c**) and 1.5 N (**b**, **d**) on quartz after magnetorheological polishing

with a deformed layer and the slip lines typical of a crystalline material on them were not presented. The tops of the imprint were rounded. Fragments of cracks were visible in the fractures of the modified layer, which at a load of 0.01 N were not even visible on the surface behind the indentation contour. With an increase in the load, the cracks break the layer, and partially peels off the surface (Fig. 4d). On the figures with absent surface layer (Fig. 4d), slip lines and cracks are visible. Thus, it can be assumed that the material is cracking, but under the layer it is not possible to reveal this from the surface.

Imprints on quartz after MRF possess a structure typical for "hard" materials (Fig. 5). The shape of the imprint is incorrect, which corresponds to the fact that the deformation pattern in an imprint on a crystal depends on the orientation of the crystal lattice with respect to the indenter (Eidel 2011). The largest crack in all imprints has a direction of 20° along the Y axis. According to (Pizzagalli et al. 2013), the crack propagates primarily in the direction of the least strength of the crystal lattice. In this case, this direction coincides with the direction of the predominant entrainment of material in Fig. 1b, d. Chips of the material follow the contour of the imprint. Among the indentation contour at 0.01 N, only one edge was straight (Fig. 5c). There were no straight edges among the imprint contour at 1.5 N (Fig. 5d). On the imprint faces there were "steps" typical of crystal slip lines (Fig. 5c, d) (Januchta and Smedskjaer 2019). In the fields of smaller size, it can be seen that at low loads, the width of the steps was greater, about 200–400 nm

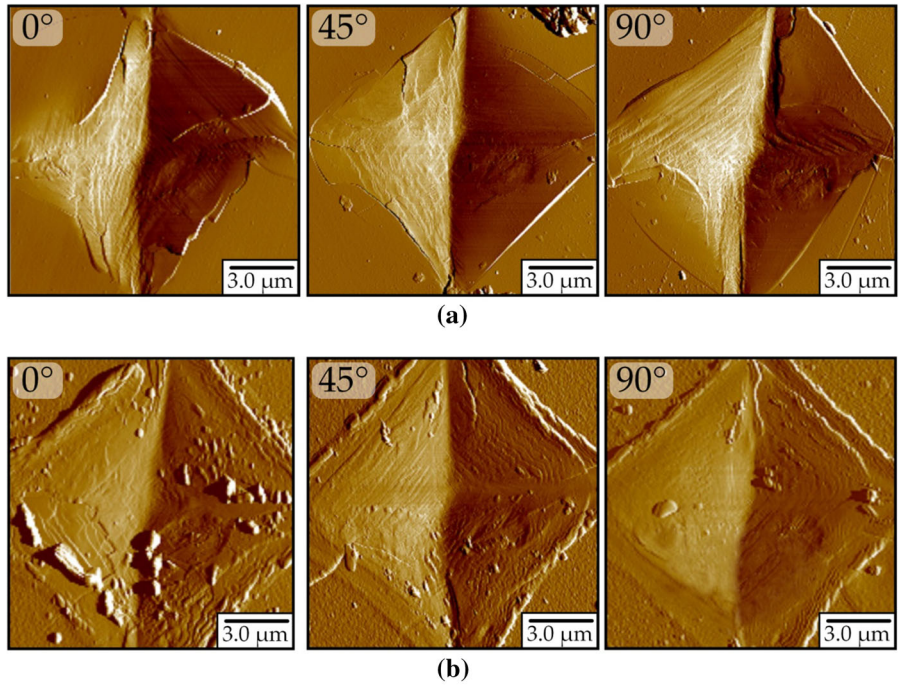

Fig. 6 Shape of Vickers indentations from the angle of rotation of quartz plates after MRF (**a**) and CMP (**b**)

Table 2 The half-diagonal length of the indentations a, the crack lengths c_1 and c_2, and the c_2 / a ratio for monocrystalline quartz plates after CMP and MRF, depending on the rotation angle

Angle (°)	a (μm)		c_1(μm)		c_2(μm)		c_2/a	
	CMP	*MRF*	*CMP*	*MRF*	*CMP*	*MRF*	*CMP*	*MRF*
0	9.46	8.21	10.21	14.64	19.70	21.16	2.08	2.58
45	9.18	7.67	12.60	10.78	21.45	17.79	2.33	2.32
90	9.22	7.97	10.91	13.24	19.41	20.41	2.11	2.56

(Fig. 5c), and with increasing load, the width decreased to 100–200 nm (Fig. 5c, d).

Since the quartz plates (disks) have a symmetrical shape without marks characterizing the orientation, the effect of the angle of rotation (0°, 45°, and 90°) of the quartz plate on the shape of the imprint, the type and length of cracks, and the magnitude of crack resistance was obtained. Rotation by 45° and 90° was performed relative to the original position, which corresponded to the imprints described above (Fig. 4c and 5c). The shape of the imprint on quartz after MRF changed significantly with the rotation angle (Fig. 6a). The most regular equilateral shape of the imprint was obtained at an angle of rotation of 45° and it was similar to the shape of the imprints obtained in (Whitney et al. 2007).

The shape of the imprint at an angle of rotation of 90° was, as in the initial one, of the curved form. In quartz after CMP under a soft modified layer, the shape of the imprints at all angles of rotation was correct and the appearance of the prints at each angle was the same (Fig. 6b). The length of cracks, depending on the angle of rotation, for quartz after MRF changed and a for quartz after CMP remained close (Table 2). To determine K_{IC}, the most suitable orientation for quartz after MRF was the initial one, since it corresponded to the longest cracks. The length of the half-diagonal of the imprint a, the lengths of cracks near c_1 and from the center of the c_2 of the indent, as well as the ratio of the length of the crack from the center of the indent to the length of the half-diagonal c_2/a are given in Table 3. The presence of a

Table 3 Diagonal length of imprints a, crack length c_1 and c_2 and the relation c_2/a

Load P (N)	a (μm)		c_1(μm)		c_2(μm)		c_2/a	
	CMP	*MRF*	*CMP*	*MRF*	*CMP*	*MRF*	*CMP*	*MRF*
0.01	4.03	3.01	2.50	3.95	5.95	6.12	1.48	2.03
0.05	4.06	2.99	2.77	4.06	6.23	6.15	1.54	2.06
0.1	3.77	3.28	2.62	4.72	5.59	7.37	1.48	2.25
0.2	4.42	3.57	2.87	5.51	6.57	8.13	1.49	2.28
0.3	4.11	3.97	3.65	5.40	7.85	8.45	1.91	2.13
0.4	5.35	4.58	4.19	6.21	9.09	9.66	1.70	2.11
0.5	6.00	4.95	4.48	6.85	9.79	10.94	1.63	2.21
0.6	6.41	5.34	5.54	8.41	11.38	12.58	1.75	2.35
0.7	6.88	5.71	6.54	8.00	12.76	12.48	1.86	2.18
0.8	7.42	6.07	7.82	9.16	14.14	14.28	1.91	2.35
0.9	7.46	6.31	7.62	9.23	14.47	14.30	1.94	2.27
1.0	7.87	6.57	8.62	9.72	15.72	14.56	2.00	2.22
1.5	9.46	8.21	10.21	14.64	19.70	21.16	2.08	2.58
2.0	10.66	9.19	12.11	16.64	22.42	22.92	2.10	2.49
2.5	11.91	10.35	15.12	20.37	26.31	29.27	2.21	2.83

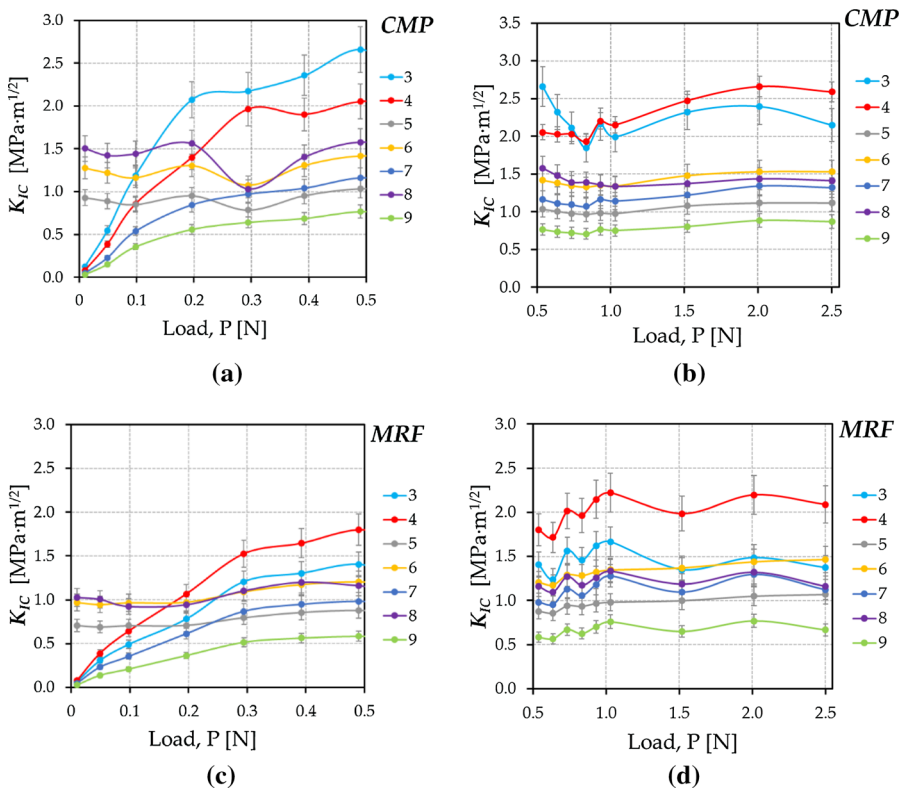

Fig. 7 Dependence of K_{IC} on the load from 0.01 to 0.5 N (**a**, **c**) and from 0.5 to 2.5 N (**b**, **d**) for quartz after chemical–mechanical polishing (**a**, **b**) and magnetorheological polishing (**c**, **d**)

layer on the quartz surface after CMP interferes with the reliable identification of the lengths of cracks on the surface of the samples. The difference between the length of cracks near the indent c_1 after CMP and MRF reaches 30%, between the length of cracks from the center of the indent up to 10%. In all the cases, the

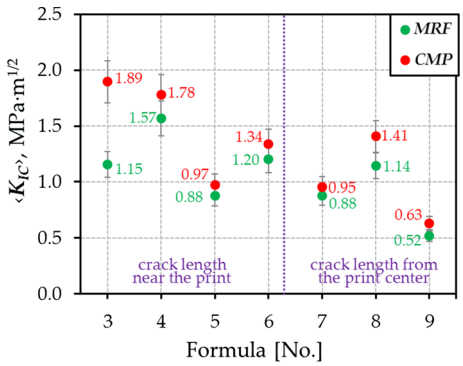

Fig. 8 Average K_{IC} values determined by formulas (3)–(9)

crack of shorter length was observed for quartz after CMP. This can affect K_{IC} values for completely identical materials and lead to significant differences in values.

The table shows that the ratios c_2/a, which is the criterion for choosing the formulas for calculating K_{IC} for quartz, differ. For quartz after CMP for loads up to 1.0 N, the calculation should be performed using the formulas (3)–(6), since the value of $c_2/a < 2.0$, and for loads above 1.0 N the value of $c_2/a > 2{,}0$ and the calculation was carried out according to the formulas (7)–(9). For quartz after MRF at all loads $c_2/a > 2.0$ and the calculation was carried out according to the formulas (7)–(9).

The K_{IC} values at low loads from 0.01 to 0.5 N determined by the formulas (3), (4), (7) and (9) proportionally depend on the applied load P (Fig. 7a, c) and with decreasing load the K_{IC} values decrease as well. At loads of 0.5 N and more, the K_{IC} values for quartz in both types of polishing are more stable and slightly change relative to the average value (Fig. 7b, d). The K_{IC} values obtained by formulas (5), (6) and (8), which do not include the load in the calculation, and in the region of low loads slightly deviate from the average value.

A significant decrease in K_{IC} values in the load range of 0.01–0.2 N did not allow to use the formulas that include load. Formulas that do not include load give consistent results over the entire load range, high to small, and average values compared to the range obtained from the no load formulas. When comparing the K_{IC} values of quartz, one should pay attention to the formula by which it was calculated, since with the same crack length and half-diagonal of the imprint, the values may differ by 4 times. At low loads less than 0.5 N, one should pay attention to the type of polishing with which its surface was treated. At loads over 1.0 N, the type of polishing does not significantly affect the K_{IC} value.

According to the average K_{IC} values determined in the area of loads above 0.5 N (Fig. 7b, d), it was obtained that the values for quartz after CMP are higher than for quartz after MRF (Fig. 8). However, this is only due to insufficient detection of the end of the crack as a result of the presence of a softer layer on quartz after CMP. The values obtained by the formulas (3), (4), and (9), which include only the crack length, half-diagonal length of the imprint and load, demonstrate a wide scatter. The values of K_{IC}, determined by the formulas (5), (6) and (8), in comparison with other formulas, are close to each other. The results of formula (7) at loads less than 0.5 N significantly depend on the load, as well as formulas (3), (4), and (9), and with decreasing load, the values of K_{IC} also decrease. At the loads above 0.5 N, the results of the formulas are close in values to those obtained by formulas (5), (6) and (8). Thus, we can propose that the formula (7) can be applied at loads of 0.5 N and higher. The values obtained by the formulas (5), (6) and (8) can be considered the most reliable ones, since

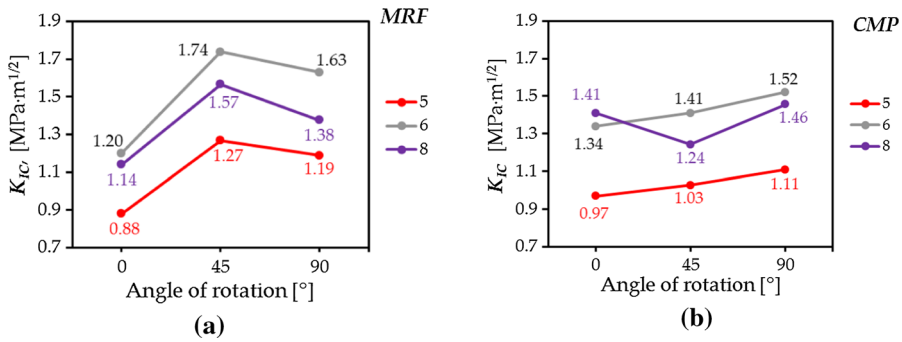

Fig. 9 Average values of K_{IC} determined by formulas (5), (6) and (8) of quartz plates after *MRF* (**a**) and *CMP* (**b**)

they are very close to the values obtained in (Whitney et al. 2007), and are close to each other. Moreover, the applicability of these formulas depends on the value of c_2/a. If Palmquist cracks are formed ($c_2/a < 2.0$), then (5) and (6) are applied, and if median cracks ($c_2/a > 2.0$), then the formula (8) is recommended.

The calculation of K_{IC} for quartz samples after two different treatments at different angles of rotation of the samples relative to the indenter was carried out according to the formulas (5), (6) and (8). It was found that since the angle of rotation affects the length of cracks at the indentation, it also affects the value of K_{IC}. At an angle of 45°, K_{IC} increases in quartz after *MRF*, and decreases in quartz after *CMP* (Fig. 9a). At an angle of 90°, the opposite is true (Fig. 9b). The K_{IC} values, depending on the angle, can vary by 20–30%, both upward and downward. Hence, we can conclude that when determining K_{IC} in a single-crystal material, one should take into account the orientation of the sample relative to the indenter, otherwise the error may amount to 20–30%.

4 Conclusions

The surface of monocrystalline quartz after two types of polishing techniques (chemical–mechanical and magnetorheological) was investigated in this work. The effect of treatment on surface morphology, roughness, elastic modulus, microhardness and crack resistance was evaluated. The criterion for crack resistance was the critical stress intensity factor K_{IC}. Various methods for calculating K_{IC} were compared in the load range from 0.01 to 2.5 N. The main conclusions are as follows:

- using AFM and NI methods, we have comprehensively described the surface morphology, physical and mechanical properties of the quartz surface after chemical–mechanical and magnetorheological polishing;
- on the surface of quartz after chemical–mechanical polishing, there is an altered layer with a thickness of 70 nm, which reduces the E and H values of the surface, hides cracks and makes it impossible to determine the true K_{IC} at loads below 1 N;
- magnetorheological polishing achieves surface roughness Ra = 0.4 nm without the presence of extraneous layers;
- it is recommended to measure K_{IC} over several indentations, using different angles of rotation of quartz samples relative to the indenter for a more accurate determination of the fracture toughness value;
- K_{IC} was determined to be 0.88–1.20 MPa $m^{1/2}$ when the specimen was oriented relative to the indenter, giving the maximum crack length, and 1.27–1.74 MPa $m^{1/2}$ when the specimen was oriented relative to the indenter, giving the minimum crack length. Differences in values associated with the orientation of the indenter relative to the quartz sample can reach 20–30%;
- when comparing K_{IC} with the literature data, one should take into account the formula by which the value and technology of quartz surface treatment were calculated. It is shown that for calculating K_{IC} one should also take into account the physical and mechanical characteristics of the material, the geometric parameters of the imprint.

Acknowledgements This research was supported by the grant of Belarusian Republican Foundation for Fundamental Research BRFFR Nos. F20M-083 and F18R-239. Evgeniy V. Sadyrin was supported by the grant of the Russian Science Foundation, Grant Number 19-19-00444.

Author contributions All authors contributed to the study conception and design. Material preparation and data collection was performed by Vasilina A. Lapitskaya and Tatyana A. Kuznetsova. Visualization of the samples was conducted by Vasilina A. Lapitskaya and Andrei L. Khudoley. Analysis of experimental data was performed by Anastasiya V. Khabarava, Sergei A. Chizhik, Vasilina A. Lapitskaya, Tatyana A. Kuznetsova and Evgeniy V. Sadyrin. Project administration was performed by Sergei M. Aizikovich. The first draft of the manuscript was written by Vasilina A. Lapitskaya and all authors commented on previous versions of the manuscript. All authors read and approved the final manuscript.

Data availability All data and materials as well as software application or custom code support the published claims and comply with field standards.

Code availability Not applicable.

Declarations

Conflict of interest The authors declare no conflict of interest.

Ethical approval Not applicable.

Consent to participate Not applicable.

Consent for publication Not applicable.

References

Anishchik V, Uglov V, Kuleshov A, Filipp A, Rusalsky D, Astashynskaya M, Samtsov M, Kuznetsova T, Thiery F, Pauleau Y (2005) Electron field emission and surface morphology of a-C and a-C: H thin films. Thin Solid Films 482:248–252. https://doi.org/10.1016/j.tsf.2004.11.153

Baek S, Kim W, Jeon S, Yong K (2018) Developing a non-optical platform for impact dynamics analysis on nanostructured superhydrophobic surfaces using a quartz crystal microbalance. Sens Actuators B Chem 262:595–602. https://doi.org/10.1016/j.snb.2018.02.031

Bai B, Li C, Zhao Y (2020) Development of v-shaped beam on the shock resistance and driving frequency of micro quartz tuning forks resonant gyroscope. Micromachines 11:1012. https://doi.org/10.3390/mi11111012

Bedi TS, Singh AK (2016) Magnetorheological methods for nanofinishing—a review. Part Sci Technol 34:412–422. https://doi.org/10.1080/02726351.2015.1081657

Beitia J, Clifford A, Fell C, Loisel P (2015) Quartz pendulous accelerometers for navigation and tactical grade systems. In: Proceedings of the 2015 DGON inertial sensors and systems, Institute of Electrical and Electronics Engineers Inc., 2015. Karlsruhe 2015, pp 1–20, https://doi.org/10.1109/InertialSensors.2015.7314256

Bo D, Jianwei Z, Yuling L, Mingbin S, Yufeng Z (2014) Surface roughness of optical quartz substrate by chemical mechanical polishing. J Semicond 35:116001. https://doi.org/10.1088/1674-4926/35/11/116001

Burlakova VE, Tyurin AI, Drogan EG, Sadyrin EV, Pirozhkova TS, Novikova AA, Belikova MA (2019) Mechanical properties and size effects of self-organized film. J Tribol 141:051601. https://doi.org/10.1115/1.4042678

Cao J, Li J, Nie M, Zhu P, Zhao C, Zhang J, Xuan T, Xu J, Li B (2019) A novel surface polishing method and its fundamental performance in ultra-fine polishing of wafer. Int J Adv Manuf Technol 105:2919–2933. https://doi.org/10.1007/s00170-019-04473-9

Cho NJ, D'Amour JN, Stalgren J, Knoll W, Kanazawa K, Frank CW (2007) Quartz resonator signatures under Newtonian liquid loading for initial instrument check. J Colloid Interface Sci 315:248–254. https://doi.org/10.1016/j.jcis.2007.06.020

Danel JS, Delapierre G (1991) Quartz: a material for microdevices. J Micromech Microeng 1:187–198. https://doi.org/10.1088/0960-1317/1/4/001

Dokou E, Zhang L, Barteau MA (2002) Comparison of atomic force microscopy imaging methods and roughness determinations for a highly polished quartz surface. J. Vac Sci Technol B Microelectron Nanom Struct 20:2183–2186. https://doi.org/10.1116/1.1513633

Dong R, Jiang X, Hao C, Xu W, Li H, Chen Y, Xie T (2019) Wettability of quartz controlled by UV light irradiation using an azobenzene surfactant. Colloids Surfaces A Physicochem Eng Asp 578:123586. https://doi.org/10.1016/j.colsurfa.2019.123586

Ebrahimi F, Kalwani L (1999) Fracture anisotropy in silicon single crystal. Mater Sci Eng A 268:116–126. https://doi.org/10.1016/S0921-5093(99)00077-5

Eidel B (2011) Crystal plasticity finite-element analysis versus experimental results of pyramidal indentation into (0 0 1) fcc single crystal. Acta Mater 59:1761–1771

Evans AG, Wilshaw TR (1976) Quasi-static solid particle damage in brittle solids-I. Observations analysis and implications. Acta Metall 24:939–956. https://doi.org/10.1016/0001-6160(76)90042-0

Ferguson CC, Lloyd GE, Knipe RJ (1987) Fracture mechanics and deformation processes in natural quartz: a combined Vickers identification, SEM, and TEM study. Can J Earth Sci 24:544–555. https://doi.org/10.1139/e87-053

Gorodkin G, Novikova Z (2012) Influence of flowing parameter of magnetorheological polishing fluids (MRPFs) on the quality of processing polycrystalline glass ceramics. J Intell Mater Syst Struct 23:959–962. https://doi.org/10.1177/1045389X11428365

Gupta MK, Rasheed IA, Suresh MB (2020) Advances in nanofinishing of optical glasses and glass ceramics. In: Handbook of advanced ceramics and composites, Springer, pp 569–599

Guzzo PL (2001) Evaluation of hardness and fracture toughness in natural quartz crystals by indentation experiments. In: 16th Brazilian congress of mechanical engineering 2:155–161

Guzzo PL, Raslan AA, De Mello JDB (2003) Ultrasonic abrasion of quartz crystals. Wear 255:67–77. https://doi.org/10.1016/S0043-1648(03)00094-2

Hampitak P, Melendrez D, Iliut M, Fresquet M, Parsons N, Spencer B, Jowitt TA, Vijayaraghavan A (2020) Protein interactions and conformations on graphene-based materials mapped using quartz-crystal microbalance with dissipation monitoring (QCM-D). Carbon N Y 165:317–327. https://doi.org/10.1016/j.carbon.2020.04.093

Hao D, Hu C, Grant J, Glidle A, Cumming DRS (2018) Hybrid localized surface plasmon resonance and quartz crystal microbalance sensor for label free biosensing. Biosens Bioelectron 100:23–27. https://doi.org/10.1016/j.bios.2017.08.038

Hildebrand J, Hecht K, Bliedtner J, Müller H (2011) Laser beam polishing of quartz glass surfaces. Phys Proc 12:452–461. https://doi.org/10.1016/j.phpro.2011.03.056

Hocheng H, Kuo KL (2002) Fundamental study of ultrasonic polishing of mold steel. Int J Mach Tools Manuf 42:7–13. https://doi.org/10.1016/S0890-6955(01)00099-2

ISO - ISO 19606:2017 Fine ceramics (advanced ceramics, advanced technical ceramics)—Test method for surface roughness of fine ceramic films by atomic force microscopy. https://www.iso.org/standard/65457.html. Accessed 4 Dec 2020

Januchta K, Smedskjaer MM (2019) Indentation deformation in oxide glasses: quantification, structural changes, and relation to cracking. J Non-Crystalline Solids X 1:100007. https://doi.org/10.1016/j.nocx.2018.100007

Jha KK, Suksawang N, Lahiri D, Agarwal A (2012) Energy-based analysis of nanoindentation curves for cementitious materials. ACI Mater J 109:81–90. https://doi.org/10.14359/51683573

Kanaev AA (2019) Effect of surface-active components of polishing compositions on the deformational-strength properties of ruby and quartz surfaces. Glas Ceram 75:435–437. https://doi.org/10.1007/s10717-019-00106-5

Khort A, Romanovski V, Lapitskaya V, Kuznetsova T, Yusupov K, Moskovskikh D, Haiduk Y, Podbolotov K (2020) Graphene@metal nanocomposites by solution combustion synthesis. Inorg Chem 59:6550–6565. https://doi.org/10.1021/acs.inorgchem.0c00673

Kim DW, Lee JW, Cho MW, Choi SB (2009) An experimental study on the ultra-precision polishing of quartz crystal using MR fluids and micro abrasives. J Phys Conf Ser 149:012061. https://doi.org/10.1088/1742-6596/149/1/012061

Kuznetsova TA, Lapitskaya VA, Chizhik SA, Uglov VV, Shymanski VI, Kvasov NT (2018) Morphology of multilayer AlN/SiN coatings with layers of different thickness. IOP Conf Ser 443:012018. https://doi.org/10.1088/1757-899X/443/1/012018

Kuznetsova T, Lapitskaya V, Khabarava A, Chizhik S, Warcholinski B, Gilewicz A (2020) The influence of nitrogen on the morphology of ZrN coatings deposited by magnetron sputtering. Appl Surf Sci. https://doi.org/10.1016/j.apsusc.2020.146508

Lamberson L, Ramesh KT (2017) Dynamic electromechanical behavior of single-crystal α-quartz. Int J Impact Eng 110:338–345. https://doi.org/10.1016/j.ijimpeng.2017.01.029

Lapitskaya VA, Kuznetsova TA, Chizhik SA, Rogachev AA (2018) Morphology of multilayer metal-carbon coatings with different arrangements of functional layers. IOP Conf Series 443(1):012020. https://doi.org/10.1088/1757-899X/443/1/012020

Lapitskaya VA, Kuznetsova TA, Chizhik SA, Komarov AI, Frolov YI, Romanyuk AS (2019) Study of the crack resistance of microarc oxidation coatings after laser doping with zirconium oxide. Tech Phys 64:1609–1614. https://doi.org/10.1134/S1063784219110173

Lapitskaya VA, Kuznetsova TA, Chizhik SA, Solovei DV, Warcholinski B, Gilevicz A, Aizikovich SM, Mitrin BI, Krenev LI (2020) Wear of thin coatings with different hardness by probe methods. J Surf Invest 14:602–608. https://doi.org/10.1134/S1027451020030325

Lawn BR, Fuller ER (1975) Equilibrium penny-like cracks in indentation fracture. J Mater Sci 10:2016–2024. https://doi.org/10.1007/BF00557479

Lawn BR, Evans AG, Marshall DB (1980) Elastic/plastic indentation damage in ceramics: the median/radial crack system. J Am Ceram Soc 63:574–581. https://doi.org/10.1111/j.1151-2916.1980.tb10768.x

Lee BM, Nam HG, Choi HY, Hong SK, Jeong YG, Choi JH (2018) Transparent electric heaters based on photoresist-derived carbon micropatterns on quartz plates. Macromol Mater Eng 303:1–7. https://doi.org/10.1002/mame.201800296

Leppin C, Hampel S, Meyer FS, Langhoff A, Fittschen UEA, Johannsmann D (2020) A quartz crystal microbalance, which tracks four overtones in parallel with a time resolution of 10 milliseconds: application to inkjet printing. Sensors 20:1–17. https://doi.org/10.3390/s20205915

Liang J, Zhang L, Wang L, Dong Y, Ueda T (2015) Flip chip bonding of a quartz MEMS-based vibrating beam accelerometer. Sensors 15:22049–22059. https://doi.org/10.3390/s150922049

Ma CP, Guan YC, Zhou W (2017) Laser polishing of additive manufactured Ti alloys. Opt Lasers Eng 93:171–177. https://doi.org/10.1016/j.optlaseng.2017.02.005

Malshe AP, Park BS, Brown WD, Naseem HA (1999) A review of techniques for polishing and planarizing chemically vapor-deposited (CVD) diamond films and substrates. Diam Relat Mater 8:1198–1213. https://doi.org/10.1016/S0925-9635(99)00088-6

Matko V, Milanovic M (2019) Highly enhanced inductance sensing performance of dual-quartz crystal converter. Sensors 19:2188. https://doi.org/10.3390/s19092188

Misumi I, Sugawara K, Kizu R, Hirai A, Gonda S (2019) Extension of the range of profile surface roughness measurements using metrological atomic force microscope. Precis Eng 56:321–329. https://doi.org/10.1016/j.precisioneng.2019.01.002

Molaei F, Siavoshi H (2020) Molecular dynamics studies of thermal conductivity and mechanical properties of single crystalline α-quartz. Solid State Commun 320:114020. https://doi.org/10.1016/j.ssc.2020.114020.5

Niihara K (1983) A fracture mechanics analysis of indentation-induced Palmqvist crack in ceramics. J Mater Sci Lett 2:221–223. https://doi.org/10.1007/BF00725625

Niihara K, Morena R, Hasselman DPH (1982) Evaluation of KIc of brittle solids by the indentation method with low crack-to-indent ratios. J Mater Sci Lett 1:13–16. https://doi.org/10.1007/BF00724706

Nikolaev AL, Mitrin BI, Sadyrin EV, Zelentsov VB, Aguiar AR, Aizikovich SM (2020) Mechanical properties of microposit S1813 thin layers. In: Aizikovich SM, Altenbach H, Eremeyev V, Swain MV, Galybin A (eds) Modeling, synthesis and fracture of advanced materials for industrial and medical applications. Springer, Cham

Oliver WC, Pharr GM (1992) An improved technique for determining hardness and elastic modulus using load and displacement sensing indentation experiments. J Mater Res 7:1564–1583. https://doi.org/10.1557/JMR.1992.1564

Pizzagalli L, Godet J, Guénolé J, Brochard S, Holmstrom E, Nordlund K, Albaret T (2013) A new parametrization of the Stillinger-Weber potential for an improved description of defects and plasticity of silicon. J Phys Condens Matter 25:055801. https://doi.org/10.1088/0953-8984/25/5/055801

Rianjanu A, Nugroho DB, Kusumaatmaja A, Roto R, Triyana K (2019) A study of quartz crystal microbalance modified with polyvinyl acetate nanofiber to differentiate short-chain alcohol isomers. Sens Bio-Sensing Res 25:100294. https://doi.org/10.1016/j.sbsr.2019.100294

Rudolph G, Hermansson A, Jönsson AS, Lipnizki F (2021) In situ real-time investigations on adsorptive membrane fouling by thermomechanical pulping process water with quartz crystal microbalance with dissipation monitoring (QCM-D). Sep Purif Technol 254:117578. https://doi.org/10.1016/j.seppur.2020.117578

Sadyrin E, Swain M, Mitrin B, Rzhepakovsky I, Nikolaev A, Irkha V, Yogina D, Lyanguzov N, Maksyukov S, Aizikovich S (2020a) Characterization of enamel and dentine about a white spot lesion: mechanical properties, mineral density. Microstruct Mol Compos Nanomater 10:1889. https://doi.org/10.3390/nano10091889

Sadyrin E, Vasiliev A, Volkov S (2020b) Mathematical modeling of experiment on Berkovich nanoindentation of ZrN coating on steel substrate. Acta Polytech CTU Proc 27:18–21. https://doi.org/10.14311/APP.2020.27.0018

Sergejev F (2006) Comparative study on indentation fracture toughness measurements of cermets and hardmetals. Euro PM 2006 Powder Metall Congr Exhib 1:43–48

Singh V (2016) Mechanical behaviour of silicon and quartz under various loading / unloading conditions by using nano-indentation technique. Int J Res Appl Sci Eng Technol 4:103–110

Trukhin AN (2019) Luminescence of natural α-quartz crystal with aluminum, alkali and noble ions impurities. J Lumin 214:116602. https://doi.org/10.1016/j.jlumin.2019.116602

Vasiliev AS, Sadyrin EV, Mitrin BI, Aizikovich SM, Nikolaev AL (2018) Nanoindentation of ZrN coatings on silicon and copper substrates. Russ Eng Res 38:735–737. https://doi.org/10.3103/S1068798X18090289

Warcholinski B, Gilewicz A, Kuprin AS, Tolmachova GN, Ovcharenko VD, Kuznetsova TA, Lapitskaya VA, Chizhik SA (2019) Comparison of mechanical and tribological properties of nitride and oxynitride coatings based on chrome and zirconium obtained by cathodic arc evaporation. J Frict Wear 40(2):163–170. https://doi.org/10.3103/S1068366619020156

Weingarten C, Schmickler A, Willenborg E, Wissenbach K, Poprawe R (2017) Laser polishing and laser shape correction of optical glass. J Laser Appl 29:011702. https://doi.org/10.2351/1.4974905

Whitney DL, Broz M, Cook RF (2007) Hardness, toughness, and modulus of some common metamorphic minerals. Am Mineral 92:281–288. https://doi.org/10.2138/am.2007.2212

Xia Z, Fang F, Ahearne E, Tao M (2020) Advances in polishing of optical freeform surfaces: a review. J Mater Process Technol 286:116828. https://doi.org/10.1016/j.jmatprotec.2020.116828

Yang X, Wang H, Peng Z, Hao J, Zhang G, Xie W, He Y (2018) Triboelectric properties of ilmenite and quartz minerals and investigation of triboelectric separation of ilmenite ore. Int J Min Sci Technol 28:223–230. https://doi.org/10.1016/j.ijmst.2018.01.003

Yu B, Li X, Dong H, Qian L (2012) Mechanical performance of friction-induced protrusive nanostructures on monocrystalline silicon and quartz. Micro Nano Lett 7:1270–1273. https://doi.org/10.1049/mnl.2012.0521

Yu X, Chen X, Ding X, Zhao XA (2018) High-stability quartz crystal resonator humidity sensor based on tuning capacitor. IEEE Trans Instrum Meas 67:715–721. https://doi.org/10.1109/TIM.2017.2784082

Yuan JL, Zhao P, Ruan J, Cao ZX, Zhao WH, Xing T (2003) Lapping and polishing process for obtaining super-smooth surfaces of quartz crystal. J Mater Process Technol 138:116–119. https://doi.org/10.1016/S0924-0136(03)00058-X

Zhao F, Zhou L, Fan Z, Dai Z (2018) Research on surface processing of quartz wafer based on magnetorheological finishing and ion beam figuring. Proc CIRP 71:496–499. https://doi.org/10.1016/j.procir.2018.05.016

Zhong ZW (2008) Recent advances in polishing of advanced materials. Mater Manuf Process 23:449–456. https://doi.org/10.1080/10426910802103486

Zhou G, Bi Y, Ma Y, Wang L, Wang X, Yu Y, Mutzke A (2019) Large current ion beam polishing and characterization of mechanically finished titanium alloy (Ti6Al4V) surface. Appl Surf Sci 476:905–913. https://doi.org/10.1016/j.apsusc.2019.01.120